It came as a surprise to early lunar sample researchers that samples from the Apollo 12 and 14 missions had very high concentrations of the suite of trace chemical elements that geochemists categorize as "incompatible." On the Moon, incompatible elements include phosphorus, the rare earth elements, and the three most important naturally occurring radioactive elements, potassium, thorium, and uranium. Lunar rocks consist mainly of four minerals. When those minerals crystallize from a magma, the incompatible elements are excluded from the solid phases and are concentrated in the liquid phase. The existence of lunar rocks with high concentrations of incompatible elements indicated that igneous differentiation of the Moon had occurred to an advanced degree and that the Moon, unlike the parent bodies of most meteorites, was not a primitive object.

Partial mapping of the lunar surface by gamma-ray spectrometers aboard Apollo orbiting command modules showed that the region in the vicinity of the Apollo 12 and 14 sites was rich in radioactive elements. However, it was not until 1998 that the first global geochemical coverage of the Moon was obtained by gamma-ray and neutron spectrometers aboard the Lunar Prospector mission (*3*–*5*). It only became apparent more than 25 years after the last Apollo mission that three of the missions, Apollos 12, 14, and 15, had landed in a region that was uniquely rich in incompatible elements compared to most regions of the Moon and that the other three missions were in near proximity to that geochemically anomalous region (see the figure).

Various lines of evidence suggest that the early Moon was largely molten. The Lunar Prospector data showed that the chemical differentiation of the Moon, as it formed its core, mantle, and crust, was asymmetric. The last liquid, by then rich in incompatible trace elements, concentrated in what is now the northwest quadrant of the nearside. One of the last and largest basin-forming impactors, the one that produced the Imbrium basin, struck this geochemically anomalous region 3.9 billion years ago, spreading thorium-rich ejecta over the surface of the Moon (*6*). All six Apollo landing sites contain rocks, mainly ancient impact-melt breccias, that are rich in thorium (typically 8 to 20 μg/g) and other incompatible elements. One interpretation is that these thorium-rich impact melt breccias were produced when the Imbrium impactor struck the incompatible-element–rich region (*7*). Another is that a cataclysmic set of impact events occurring within a short interval about 3.9 billion years ago produced all of the major nearside lunar basins and that several of those impacts excavated high-thorium material (*8*). Unlike typical rocks from the Apollo sites, most lunar meteorites, including ALHA 81005, have low concentrations of thorium, typically less than 1 μg/g. These low-thorium meteorites must originate from the vast portions of the Moon, mainly on the farside, with low surface concentrations of thorium (*9*).

SaU 169 represents the opposite extreme. It is an impact-melt breccia with exceedingly high concentrations of thorium (33 μg/g) and other incompatible elements. As Gnos *et al*. argue, SaU 169 almost certainly originates from within the high-thorium anomaly. If lunar meteorites are random samples of the Moon, it was predictable that sooner or later a high-thorium lunar meteorite would be found. It is nevertheless ironic that even though the Apollo missions inadvertently visited some of the most thorium-rich areas of the Moon, SaU 169 is richer in incompatible elements than any rock-sized Apollo sample.

The most significant aspect of the work of Gnos *et al*. is the ^{207}Pb-^{206}Pb crystallization age of 3.909 ± 0.009 billion years that they obtain for the impact melt on the basis of ion microprobe analysis of zircons. They conclude that this age precisely dates the Imbrium impact, although the age is significantly older than the previous best working ages of 3.85 ± 0.02 billion years (*8*) for Imbrium and 3.89 ± 0.01 billion years for the Serenitatis basin (*10*). The data for SaU 169 call into question just which isotopic systems best record the crystallization age of an impact melt and whether the small differences (<2%) in ^{40}Ar-^{39}Ar ages among ancient impact-melt rocks are significant. It is now imperative that ^{207}Pb-^{206}Pb ages be obtained from zircons in thorium-rich melt breccias from the Apollo landing sites for comparison.

References

1. U. B. Marvin, *Geophys. Res. Lett.* **10**, 775 (1983).
2. E. Gnos *et al*., *Science* **305**, 657 (2004).
3. D. J. Lawrence *et al*., *Science* **281**, 1484 (1998).
4. R. C. Elphic *et al*., *J. Geophys. Res.* **105**, 20333 (2000).
5. D. J. Lawrence *et al*., *J. Geophys. Res.* **108**, 5102, 10.1029/2003JE002050 (2003).
6. L. A. Haskin, *J. Geophys. Res.* **103**, 1679 (1998).
7. L. A. Haskin *et al*., *Meteorit. Planet. Sci.* **33**, 959 (1998).
8. G. Ryder, *J. Geophys. Res.* **107**, 6-1, 10.1029/2001JE001583 (2002).
9. R. L. Korotev *et al*., *Geochim. Cosmochim. Acta* **67**, 4895 (2003).
10. G. B. Dalrymple, G. Ryder, *J. Geophys. Res.* **101**, 26069 (1996).

MATERIALS SCIENCE

Watching the Nanograins Roll

E. Ma

Conventional engineering materials are usually polycrystalline solids composed of crystallites (grains) that are many micrometers in diameter (*d*). The recent advent of nanocrystalline materials, for which *d* is less than 100 nm, has opened new opportunities for research and applications. For the "upper nano" regime with $d \approx$ 100 nm, research on mechanical properties has focused on tailoring the grain and/or boundary structures for optimized strength and ductility (*1*). The "lower nano" regime with $d <$ ~30 nm, on the other hand, is the realm for discovery of new deformation mechanisms (*2*–*13*). This is because the nucleation and movement of line defects called dislocations—the main carrier of plastic deformation in coarse-grained metals—is projected to be difficult in such tiny grains where the distance between dislocation pinning points becomes very small, demanding very high stresses to activate dislocation sources. Deformation processes governed by abundant grain boundaries may become important, as demonstrated in nanocrystalline nickel by Shan *et al*. on page 654 of this issue (*2*). Using an in situ dark-field transmission electron microscopy (TEM) technique, the authors recorded the frequent rotation of nanocrystals ($d \approx$ 6 nm) into larger aggregates of neighboring grains during deformation.

In general, a deforming grain is forced to rotate in response to the external stresses exerted upon it by its neighbors. For conventional metals, grain rotation during deformation often accompanies the formation of texture (preferred orientation) and is accomplished by the microscopic dislocation glide on multiple active slip systems in the grains. Such extensive dislocation activity is unlikely in 6-nm grains, and texturing was not observed in heavily cold-rolled nanocrystalline palladium (*12*). Grain rotation can also be caused by extensive grain boundary sliding and diffusion, which usually occur only at elevated temperatures. But molecular dynamics (MD) computer simulations predict that such a mechanism will become operative and even dominant when *d* is reduced to ~10 nm (*4*, *7*, *8*). Evidence for this has been sought for many

The author is in the Department of Materials Science and Engineering, Johns Hopkins University, Baltimore, MD 21218, USA. E-mail: ema@jhu.edu

years, but direct experimental confirmation remained elusive except in extremely thin (~20 nm) films used for high-resolution TEM experiments (*3*).

The experimental findings of Shan *et al*. (*2*) are also valuable because our understanding of the deformation mechanisms of nanocrystalline metals has relied heavily on MD simulations. With high loads and extreme strain rates applied to produce a measurable strain within the subnanosecond MD time scale, the simulations may exclude certain time-dependent processes and cannot determine the true rate-limiting processes in real-world experiments. The MD results are sources of inspiration and guidance but do not directly validate or disprove the existence of a mechanism (*4*, *9*).

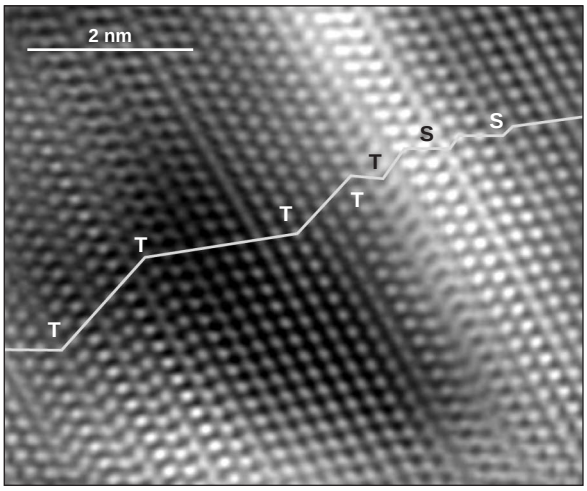

Deformation debris. An example of features left by partial dislocation–mediated processes during deformation [adapted from (*6*)]. A Fourier-filtered high-resolution TEM shows the stacking faults (S) and deformation twins (T) in a deformed nanocrystalline aluminum grain (*6*). Note the mirror symmetry across the twin boundaries, where deposited partial dislocations are also observed.

Taken together, recent TEM observations (*2*, *4*–*6*), in situ synchrotron x-ray diffraction (XRD) experiments (*10*), and advances in MD simulations begin to paint a unifying picture for the unusual deformation mechanisms in nanocrystalline face-centered-cubic metals (such as nickel and copper) (*7*, *11*). When dislocations are still involved, their operation takes different forms. First, the intragrain Frank-Read dislocation sources dominant in conventional polycrystals cease to control deformation. Instead, dislocations are nucleated out of grain boundary (GB) sources. There is also indirect evidence, including the increased strain rate sensitivity and unusually low activation volume, that hints at the defect (boundary)–assisted nucleation of dislocations as the thermally activated rate-controlling process (*14*). For *d* on the order of 30 nm, the dislocations traverse the grain and disappear into the opposing GBs, with little chance of storage inside the grains (*4*, *5*). Second, partial dislocation emission from a GB becomes more favored at sufficiently small *d*. Indeed, estimates showed that the energy cost for the nucleation of one partial dislocation at a time, which is observed in MD simulations for all the nanocrystalline metals studied (including those with high stacking fault energy) (*7*, *9*), can be lower than that for emitting a full (perfect) dislocation (*6*). The partial dislocation–mediated processes do leave behind debris, such as the stacking faults and deformation twins in the figure (*6*, *12, 15*), that can be observed in postmortem TEM. However, the nucleation of a trailing partial dislocation on the same plane of an existing leading partial dislocation, before the latter gets absorbed by the opposing GB, is often possible and can be an energetically less expensive process than other options [such as the emission of a second partial dislocation on the adjacent plane for twin nucleation (*9*)]. The trailing partial dislocation then erases the stacking fault and may catch up with the leading partial dislocation. The resulting full dislocations are not often observed in TEM, as they leave no footprint in their wake after traversing the grain. Their action was inferred from the in situ XRD measurements (*10*). It is interesting that a unit dislocation trapped inside the grain under loading has been captured by Shan *et al.* (*2*).

Large stresses are required to drive deformation in nanoscale grains. The local stress intensity can be particularly high and varied depending on loading conditions, such that one may observe all types of slip: extended partial dislocations forming stacking faults, full dislocations, and deformation twinning (*6*, *9*). Note that dislocation activities persist even when *d* is reduced down to ~10 nm (*2*, *6*, *12*, *15*). At such small grain sizes, GB sliding and grain rotation become detectable, concurrent with dislocation activities and possibly also accommodated by atomic shuffling at the GBs (*4*). A supporting finding for the active role of grain rotation and GB sliding, as directly observed by Shan *et al*., is the lack of crystallographic texture in nanocrystalline palladium grains that remained equiaxed even after large plastic deformation (*12*). Rosner *et al*. also suggest that the number of glide systems active in the coplanar twinning they observed is obviously short of the five slip systems required for a general deformation in polycrystals (*12*).

Simulations with idealized samples have predicted predominant GB sliding at $d <$ ~10 nm (*7*), but the experimental samples available so far [see figure 1 of Shan *et al*. (*2*)] always contain a grain size distribution and some impurities, with a large (number and volume) fraction of the grains larger than 10 nm. Some deposited grains in columnar shape also may not be conducive to GB sliding and grain rotation. As a result, GB–mediated plasticity may be a contributing but not yet dominant mechanism. The Hall-Petch relationship (increasing strength with decreasing *d*) may continue to hold for the nickel films of Shan *et al*. (*13*) without displaying an obvious maximum strength beyond which an inverse Hall-Petch behavior (softening) takes over (*7*).

Grain rotation and GB sliding, with no evidence of dislocation activities, were thought to control deformation in gold films with $d = 10$ nm (*3*), but the sample used was ultrathin (10 to 20 nm) and the deformation rate was very slow. In this case, the two-dimensional geometry lacks the three-dimensional constraints and has a very high surface-to-volume ratio. This accentuates the thermally activated processes facilitating grain rotation, such as diffusion, especially when under electron irradiation in TEM. Note that even the thicker films of Shan *et al*. are not free of such effects (*16*), even though the authors believe that the surface effects and stress-assisted grain growth (due to driving forces to reduce surface or GB energy) are negligible (*2*). Therefore, although the result of Shan *et al*. brings new insight into the deformation of extremely small grains, caution should be exercised before generalizing the behavior in TEM foils as fully representative of bulk deformation.

References and Notes

1. Y. M. Wang *et al.*, *Nature* **419**, 912 (2002).
2. Z. Shan *et al.*, *Science* **305**, 654 (2004).
3. M. Ke *et al.*, *Nanostruct. Mater.* **5**, 689 (1995).
4. K. S. Kumar, H. Van Swygenhoven, S. Suresh, *Acta Mater.* **51**, 387 (2003).
5. R. C. Hugo *et al.*, *Acta Mater.* **51**, 1937 (2003).
6. M. W. Chen *et al.*, *Science* **300**, 1275 (2003).
7. J. Schiotz, K. W. Jacobsen, *Science* **301**, 1357 (2003).
8. V. Yamakov *et al.*, *Nature Mater.* **3**, 43 (2004).
9. H. Van Swygenhoven *et al.*, *Nature Mater.* **3**, 399 (2004).
10. Z. Budrovic *et al.*, *Science* **304**, 273 (2004).
11. S. Cheng *et al.*, *Acta Mater.* **51**, 4505 (2003).
12. H. Rosner *et al.*, *Philos. Mag. Lett.* **84**, 321 (2004).
13. J. A. Knapp, D. M. Follstaedt, *J. Mater. Res.* **19**, 218 (2004).
14. Our stress relaxation and jump tests for nickel with d = 30 nm showed a room-temperature strain rate sensitivity four times that of coarse-grained nickel and an activation volume as small as 7 to 20 b^3, where b is the Burgers vector.
15. X. Z. Liao *et al.*, *Appl. Phys. Lett.* **84**, 592 (2004).
16. P. M. Derlet *et al.*, *Philos. Mag. A* **82**, 1 (2002).